2019-04-23

Structurereactivity relations in Ru catalysed furfural hydrogenation

Durndell, Lee

10.1002/cctc.201900481
ChemCatChem
Wiley

Heterogeneous & Homogeneous & Bio- & Nano-
CHEMCATCHEM
CATALYSIS

Accepted Article

Title: Structure-reactivity relations in Ru catalysed furfural hydrogenation

Authors: Lee Durndell, Guchu Zou, Wenfeng Shangguan, Adam Lee, and Karen Wilson

To be cited as: *ChemCatChem* 10.1002/cctc.201900481

Link to VoR: http://dx.doi.org/10.1002/cctc.201900481

A Journal of
ChemPubSoc Europe

WILEY-VCH

www.chemcatchem.org

WILEY-VCH

FULL PAPER

Structure-reactivity relations in Ru catalysed furfural hydrogenation

Lee J. Durndell,[a] Guchu Zou,[b] Wenfeng Shangguan,[b] Adam F. Lee[c] and Karen Wilson*[c]

Abstract: Furfural is an abundant and low-cost bio-derived platform chemical, obtained by xylose dehydration, and an important precursor to furfuryl alcohol and furan resins. The liquid phase selective hydrogenation of furfural to furfuryl alcohol was systematically investigated over silica supported Ru nanoparticles to elucidate structure-reactivity relations and obtain mechanistic insight. Furfural hydrogenation to furfuryl alcohol is weakly structure sensitive for Ru nanoparticles spanning 2 to 25 nm, and the dominant reaction pathway reaching 95 % selectivity under our conditions (<25 bar H_2 and 100-165 °C). In contrast, furfural decarbonylation to furan exhibits a strong structure sensitivity, being favored over sub-10 nm particles. Increasing pH_2 from 10 to 25 bar resulted in a modest increase in C=O hydrogenation, while higher temperatures promoted ring-opening of furfuryl alcohol.

Introduction

The global human population is expected to surpass 8.5 billion by 2030,[1] driving the development of sustainable low carbon processes to supplant fossil fuel use for chemical manufacturing and energy production.[2] The bio-refinery concept[3] is widely advanced as a means to produce sustainable fuels and chemicals from non-fossil feedstocks, but requires new catalytic processes for the selective transformation of biomass-derived oxygenates.[4] One such oxygenate, furfural, an α,β-unsaturated aldehyde, was identified in a 2004 DOE report as a key platform chemical for lignocellulose valorisation.[5] Furfural is obtained from the arabinose and xylose components of hemicellulose, either by solvothermal processing or acid dehydration of agricultural and forestry residues such as corn stover, straw, and wood fellings.[6] The chemoselective hydrogenation of furfural to furfuryl alcohol[7] provides access to a key chemical intermediate for the synthesis of high-value products including methylfuran,[8] levulinic acid,[9] γ-valerolactone (GVL),[10] and various resins and lubricants (**Scheme 1**).[11] Approximately 200,000 tonnes of furfural (62 % of global production) is converted to furfuryl alcohol annually[12] over copper chromite ($CuCr_2O_4.CuO$) catalysts[13] under forcing reaction conditions of 130-200 °C and 30 bar H_2.[13-14] This is problematic due to the acute toxicity of waste chromium compounds,[15] and the high operating costs.[16]

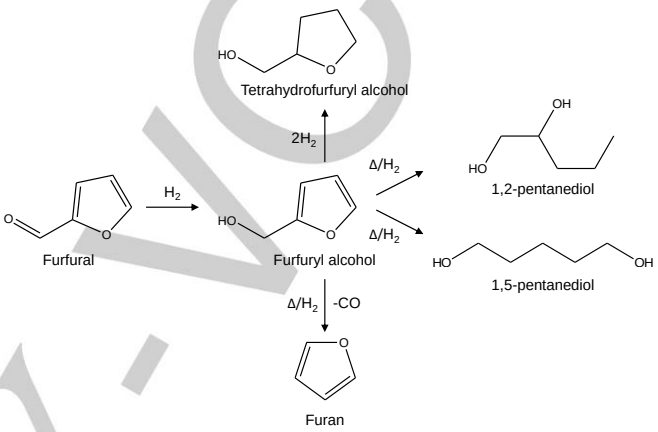

Scheme 1. Reaction network for the hydrogenation of furfural to furfuryl alcohol illustrating decarbonylation, ring opening and ring hydrogenation pathways.[17]

Transition metal catalysts have been investigated for the liquid and gas phase hydrogenation of furfural, including Pt, Pd, Ni, Ru and Cu nanoparticles (NPs).[7a, 18] Aqueous-phase furfural hydrogenation is reported over carbon supported Ru and RuSn NPs.[19] Selectivity to furfuryl alcohol decreased with reaction time from a high initial value of 99 %, due to competing ring hydrogenation and polymerisation which resulted in significant deactivation on catalyst recycling, a likely consequence of the high reaction temperature. Mironenko et al. likewise observed poor activity for aqueous phase furfural hydrogenation over Ru NPs on carbon nanotubes and carbon black, albeit under more mild reaction conditions (50 °C, 5 bar H_2) and attributed to strong water adsorption.[20] Furfuryl alcohol selectivity is broadly independent of support, and exceeds 85 %, for aqueous phase hydrogenation under mild conditions: 2 wt% Ru NPs over SiO_2, ZrO_2, and Al_2O_3 (under mild conditions of 30 °C and 5 bar H_2);[21] 5 wt% Ru NPs over MgO, hydrotalcite, activated carbon, and CaO (at 110 °C and 4 bar H_2);[22] 3 wt% Ru NPs dispersed within Zr- and Al-containing MOFs (20 °C and 5 bar H_2);[23] 4 wt% Ru over graphene oxides.[24] However, in all cases, such mild operating conditions result in low activity for furfural conversion, for which a weak particle size dependence is postulated over oxide supports.[21] To our knowledge there remain no systematic studies of particle size effects in Ru catalysed furfural hydrogenation.

Herein, we report structure-reactivity relations for the liquid phase hydrogenation of furfural over Ru NPs on silica supports. Selective hydrogenation of furfural to furfuryl alcohol, and competing decarbonylation to furan, are both structure sensitive.

[a] Dr. L. J. Durndell
School of Geography, Earth and Environmental Sciences, Faculty of Science and Engineering, University of Plymouth, Portland Square, Drake Circus, Plymouth, PL4 8AA, United Kingdom
E-mail: lee.durndell@plymouth.ac.uk
[b] Dr G. Zhou and Prof Wengfeng Shangguan
School of Mechanical Engineering, Shanghai Jiao Tong University, Shanghai, China.
[c] Prof A. F. Lee and Prof K. Wilson
Applied Chemistry & Environmental Science, School of Science, RMIT University, Melbourne VIC 3000, Australia.
E-mail: karen.wilson2@rmit.edu.au

Supporting information for this article is given via a link at the end of the document.

Results and Discussion

Catalyst characterisation

Ru NPs supported on fumed silica (Ru/SiO_2) and SBA-15 (Ru/SBA-15) were characterised by XRD, HRTEM, H_2 chemisorption and N_2 porosimetry. Low-angle XRD of the parent SBA-15[25] showed peaks at 2θ = 0.96º, 1.57º and 1.80º, corresponding to the (100), (110), and (200) reflections of an ordered hexagonal pore network with *p6mm* symmetry and a pore separation of 10.4 nm (**Figure S1**); this pore structure was retained following impregnation with Ru. N_2 porosimetry of Ru/SBA-15 samples showed Type IV adsorption isotherms and H1 hysteresis loops (**Figures S2-3**), characteristic of the SBA-15 support, for all Ru loadings. A common mean BJH pore diameter of 5.8 nm was also observed (**Figure S4**), confirming negligible mesopore blockage occurred during Ru impregnation. Fumed SiO_2 and Ru/SiO_2 samples exhibited Type II adsorption isotherms, consistent with materials comprising agglomerates of non-porous primary SiO_2 particles. BET surface areas for both silica families decreased significantly with Ru loading (**Figure 1a** and **Table S1**), with the Ru/SBA-15 materials losing up to 38 % of the parent support area. Surface area losses are attributed to partial blockage of micropores within the walls of SBA-15 upon Ru impregnation. In contrast, Ru/SiO_2 catalysts show only a small decrease in surface area, consistent with Ru NP deposition over the external surface of the amorphous support.

Wide angle XRD patterns of Ru/SiO_2 and Ru/SBA-15 confirmed the presence of hcp Ru metal (**Figure S5**),[26] with reflections observed at 2θ = 38.4º, 42.2º, 44.0º, 58.4º, 69.5º and 78.4º attributed to (100), (002), (101), (102), (210) and (103) planes.[26-27] The full-width half maximum of these reflections decreased with increasing Ru loading from 0.08 to 9.89 wt% for both silica supports, indicative of NP growth. Corresponding Ru NP sizes were quantified by Scherrer analysis (**Table S1 and Figure 1b**) revealing an increase in volume averaged particle diameters from 2.3 to 19.8 nm (over SBA-15) and 7.7 to 24.0 nm (over SiO_2); in close agreement with values from HRTEM (**Table S1**, **Figures S6-7**). Comparable Ru loadings therefore result in smaller NPs over the higher area SBA-15 than fumed silica support (**Figure 1b**), also consistent with metal dispersions obtained from H_2 pulse chemisorption (**Table S1**). Such observations are consistent with previous reports of Ni, Pd and Pt NPs impregnated over fumed silica and SBA-15 supports.[28]

Furfural hydrogenation.

The catalytic performance of Ru/SiO_2 and Ru/SBA-15 was first evaluated in furfural hydrogenation at 100 °C and 10 or 25 bar H_2. To ensure that intrinsic reaction kinetics were measured, the effect of stirrer speed on initial rate (**Figure S8**) was examined to ensure that bulk mass transport was optimal, evidenced by a plateau in the Ru surface area normalized activity (turnover frequency, TOF) for furfural hydrogenation at speeds >800 rpm. The catalyst:reactant ratio was also varied (at 900 rpm) for 0.49 and 4.05 wt% Ru/SiO_2 catalysts to confirm that the specific activities of both catalysts was zero order with respect to catalyst mass (**Figure S9**), and hence that reactions were free from bulk diffusion limitations.

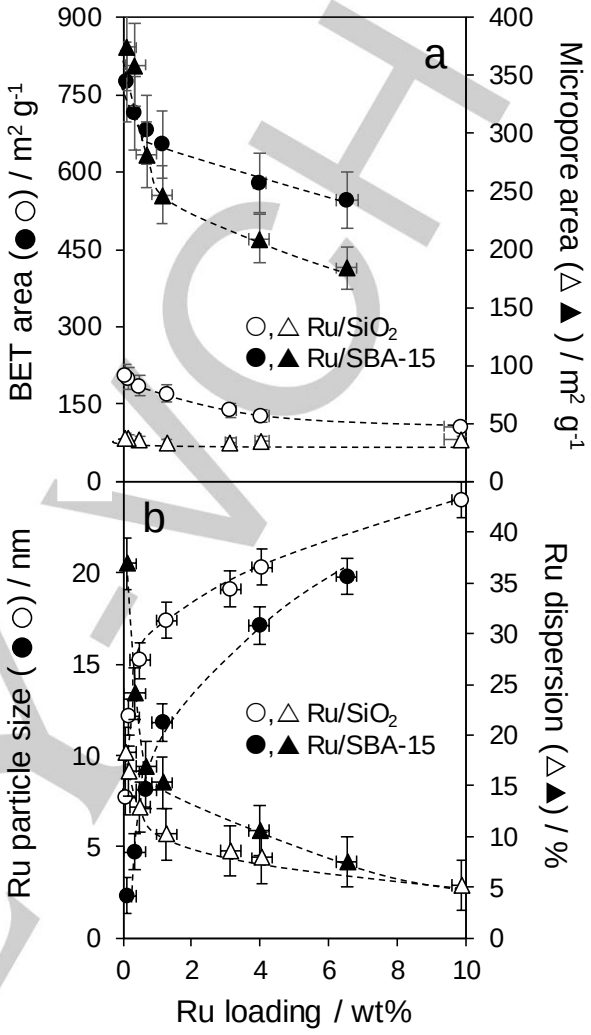

Figure 1. Impact of Ru loading on (a) BET and micropore surface areas, and (b) Ru particle size from XRD Scherrer analysis and dispersion from H_2 chemisorption measurements of Ru/SiO_2 and Ru/SBA-15.

Furfural conversion increased with Ru loading and H_2 pressure (**Figure S10**) reaching 75 % conversion after 5 h reaction at 25 bar H_2 over 9.89 wt% Ru/SiO_2. Specific (mass normalized) activities for furfural conversion were inversely proportional to Ru particle size (**Figure S11**), following the general relation rate $\propto$ (diameter)$^{-y}$. The fitted exponent was ~1 at 10 and 25 bar H_2, and for SiO_2 and SBA-15 supports, demonstrating that furfural conversion is directly proportional to the surface fraction of Ru, indicative of apparent structure insensitivity. The highest specific activities for furfural conversion of 881 (10 bar) and 1208 (25 bar) $mmol.g._{Ru}^{-1}.h^{-1}$ were observed for the smallest 2.3 nm Ru NPs. These rates are significantly higher than aqueous phase activities of 210 and 648 $mmol.g._{Ru}^{-1}.h^{-1}$ reported for Ru/C and RuSn respectively at 90 °C and 12.5 bar H_2 over similar size particles.[19] This rate enhancement is attributed to our use of toluene versus water as a solvent; the latter is postulated to irreversibly adsorb

over Ru NPs,[20] and promote the formation of water-insoluble surface polymers,[29] thereby blocking active sites. For particles >5 nm, furfural conversion was approximately first order in pH_2, reflecting the dominance of hydrogenation reaction pathways (see below). Corresponding TOFs based on furfural conversion were 380 h^{-1} (10 bar) and 850 h^{-1} (25 bar), and invariant across the Ru particle size range investigated (**Figure 2a**), again indicative of apparent structure insensitivity.

The primary products of furfural hydrogenation were furfuryl alcohol and furan, whose Ru particle size dependent production mirrors that of furfural conversion (**Figure S12**). Furfuryl alcohol productivity increased linearly with H_2 pressure for Ru particle >5 nm, associated with the increase in furfural conversion. In contrast, furan productivity was independent of H_2 pressure, consistent with a decarbonylation pathway (that does not require hydrogen).

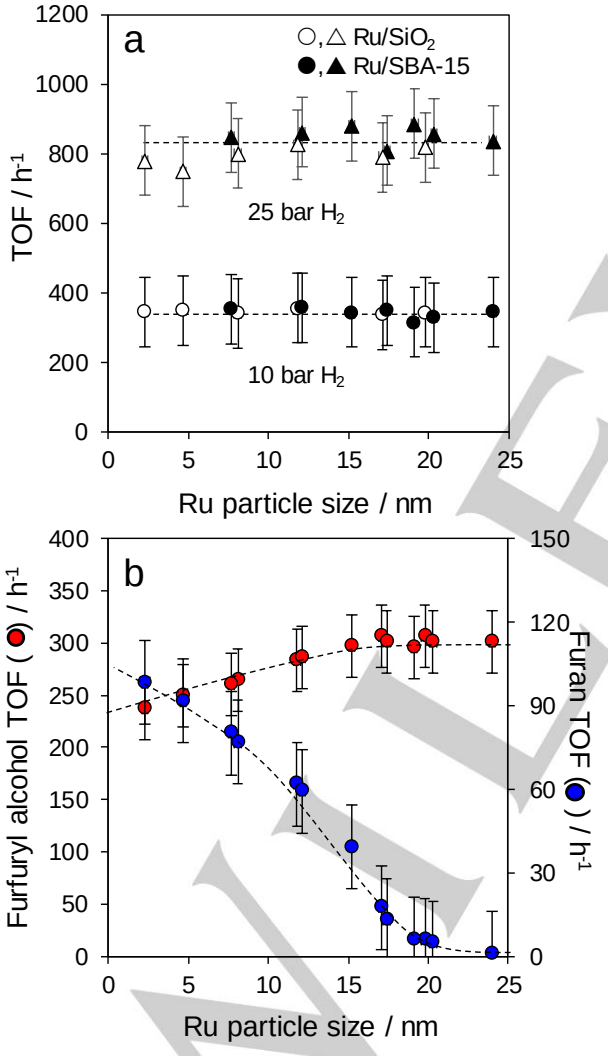

Figure 2. Turnover frequencies for (a) furfural hydrogenation at 10 and 25 bar H_2 pressure, and (b) furfuryl alcohol and furan production at 10 bar over silica supported Ru catalysts. Reaction conditions: 100 mg catalyst, 10.86 mmol furfural in 50 cm^3 toluene, 900 rpm and 100°C.

TOFs for furfuryl alcohol formation increased from 237 to 307 h^{-1} with increasing Ru particle size at 10 bar H_2, evidencing a weak structure sensitivity (**Figure 2b**). TOFs for furan production exhibited a stronger structure sensitivity, decreasing from 98 to 1 h^{-1} with increasing particle size. Similar trends were observed at 25 bar H_2 (albeit accompanied by an ~2.5-fold increase in TOFs for furfuryl alcohol formation, **Figure S13**), whereas the TOFs for furan formation show minimal pressure dependence, as expected. The observed decrease in furan productivity with Ru NP size suggests that furfural decarbonylation is favored by coordinatively unsaturated corner and edges sites, as observed for Pt NPs.[17a] Such sites may promote an η^2(C=O) binding mode, implicated as a precursor to strongly bound surface acyls (a prerequisite to decarbonylation).[30] The preceding activity measurements indicate that furfural conversion is structure insensitive over Ru NPs, in contrast to both major products. This discrepancy can be rationalised by either: (i) invoking an initial structure insensitive activation step that yields a common surface intermediate that subsequently undergoes competing structure sensitive hydrogenation or decarbonylation;[31] or (ii) a compensation effect in which furfuryl alcohol and furan both form directly from furfural, but due to their opposing structure sensitivities, net TOFs for furfural conversion remain particle size independent. Apparent activation energies for furan and furfural alcohol formation (**Figure 3**) provide some evidence for the latter hypothesis. Barriers for furfural hydrogenation fell from 29 to 14 kJ.mol^{-1} for particles >12 nm, while those for furfural decarbonylation exhibited an equal but opposite increase from 30 to 46 kJ.mol^{-1} for particles > 15 nm. The falling barrier for hydrogenation (the dominant pathway) is anticipated to have a comparatively small impact at 100 °C due to the corresponding decrease in Ru particle dispersion (number of active sites), while the concomitant rise in barrier for furan is expected to dramatically suppress its formation.

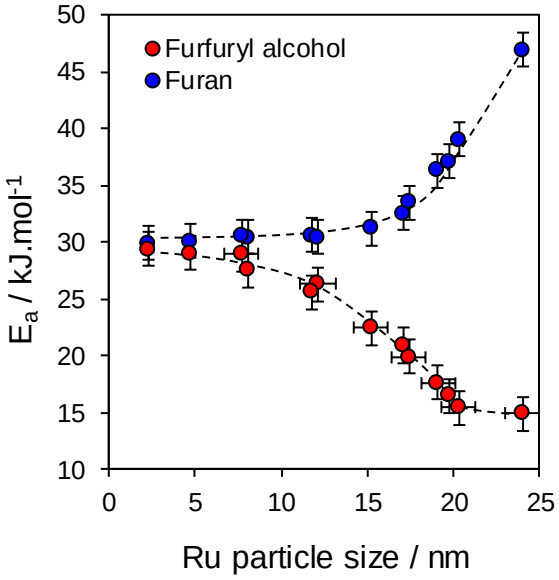

Figure 3. Influence of Ru particle size on apparent activation energy for furfural hydrogenation over silica supported Ru catalysts. Reaction conditions: 100 mg catalyst, 10.86 mmol furfural in 50 cm^3 toluene, 10 bar H_2, 900 rpm and 100-165 °C.

Consequently, the small increase in furfuryl alcohol TOFs is balanced out by the (proportionally larger) decrease in furan TOFs. Product selectivities at iso-conversion mirror their corresponding TOFs, with furfuryl alcohol favoured over larger particles at the expense of furan (**Figure 4**), and at higher hydrogen pressure, reaching ~98 selectivity to the alcohol for Ru NPs ≥17 nm. A similar size dependent selectivity is reported furfural hydrogenation over Pt NPs[17a] and for cinnamaldehyde hydrogenation to cinnamyl alcohol over carbon supported Ru NPs spanning 3-17 nm.[32] Increasing the reaction temperature to 165 °C induced a small amount (10 %) of furfuryl alcohol to undergo ring-opening and concomitant 1,2-pentandiol formation (**Figure S14**).[33]

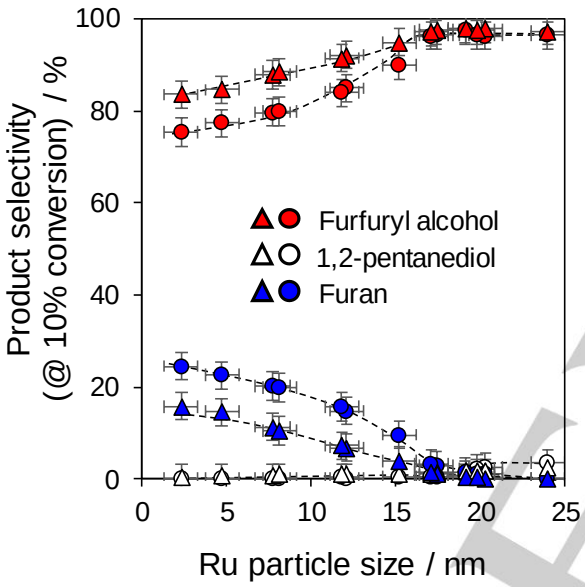

Figure 4. Influence of Ru particle size on product selectivity (at 10 % iso-conversion) for furfural hydrogenation over silica supported Ru nanoparticles at 10 bar (circles) and 25 bar H_2 (triangles). Reaction conditions: 100 mg catalyst, 10.86 mmol furfural in 50 cm^3 toluene, 900 rpm and 100 °C.

The broader potential application of silica supported Ru NPs for the selective C=O hydrogenation of biomass-derived aldehydes was subsequently demonstrated for the 4.05 wt% Ru/SiO_2 catalyst (**Table 1** and **Figure S15**). Aromatic aldehydes (benzaldehyde and vanillin) exhibited good selectivities to their corresponding unsaturated alcohols. However, allylic aldehydes (cinnamaldehyde and crotonaldehyde) exhibited lower selectivities of ~60 %, similar to those reported at 60 °C over Ru/C[32] and Ru/Al_2O_3,[34] which reflecting competing C=C hydrogenation as observed over silica supported Pt NPs.[28c]

Table 1. Performance of 4.05 wt% Ru/SiO_2 towards the hydrogenation of unsaturated aldehydes to the corresponding alcohol.

Reactant	Conversion / %[a]	Alcohol selectivity / %[b]	TOF / h^{-1}[c]
Benzaldehyde	100	99	1317
Cinnamaldehyde	68	54	740
Crotonaldehyde	43	65	455
Furfural	48	91	356
Vanillin	24	75	393

[a] Conversion at 5 h; [b] unsaturated alcohol selectivity at 5 h. Reaction conditions: 100 mg catalyst, 10.86 mmol reactant in 50 cm^3 toluene, 10 bar H_2, 900 rpm and 100 °C; [c] turnover frequencies calculated as the initial reaction rate divided by the number of moles of surface metal (based on the initial particle size and dispersion).

Conclusions

Structure-activity relationships were investigated for the liquid phase hydrogenation of furfural to furfuryl alcohol over silica supported (2-25 nm) Ru nanoparticles. Furfural conversion is directly proportional to the surface fraction of Ru, indicative of apparent structure sensitivity. Furfuryl alcohol and competing furfural decarbonylation to furan exhibit opposing structure-sensitivities; C=O hydrogenation is favored by Ru nanoparticles (>17 nm), whereas furan is favoured by sub-17 nm Ru NPs, independent of the support textural properties. These trends correlate with the diverging apparent activation energies for the hydrogenation versus decarbonylation. Increasing the pH_2 from 10 to 25 bar promotes C=O hydrogenation but has negligible impact on furan formation. Furfuryl alcohol selectivity reaches 98 % at 100 °C and 25 bar, decreasing slightly at higher temperature due to a small degree of ring-opening to 1,2-pentanediol.

Experimental Section

Catalyst synthesis

Preparation of SBA-15: SBA-15 was prepared adapting the method of Zhao et al.[25] Pluronic P123 (10 g) was dissolved in water (75.5 cm^3) and hydrochloric acid (2 M, 291.5 cm^3) with stirring at 35 °C. Tetraethylorthosilicate (15.5 cm^3) was added and left for 20 h with agitation. The resulting gel was aged for 24 h at 80 °C without agitation. The solid was filtered, washed with water (1000 cm^3) and dried at room temp before calcination at 500 °C for 6 h in air (heating ramp 1 °C.min^{-1}). The resulting silica possessed hexagonally close-packed mesopores of *p6mm* symmetry.

Preparation of Ru/SiO_2 and Ru/SBA-15: Wet impregnation of 2 g of mesoporous SBA-15 silica, and a commercial fumed silica (Sigma Aldrich S5505, 200 $m^2.g^{-1}$), was performed with 16 cm^3 aqueous Ruthenium (III) chloride solution (precursor concentrations adjusted to achieve nominal

Ru loadings of 0.05-10 wt%). The resulting slurries were stirred for 18 h at room temperature before heating to 50 °C to slowly evaporate the solvent. After a further 5 h agitation, stirring ceased, and the solids were held at 50 °C for 24 h to obtain dry powders. Finally the solids were calcined at 500 °C (ramp rate 1 °C.min^{-1}) for 2 h in static air, prior to reduction at 400 °C (ramp rate 10 °C.min^{-1}) for 2 h under 10 cm^3.min^{-1} flowing hydrogen.

Catalyst characterisation

Nitrogen porosimetry was undertaken on a Quantachrome Nova 2000e porosimeter using NovaWin version 11 analysis software. Samples were degassed at 120 °C for 2 h prior to nitrogen physisorption. Adsorption/desorption isotherms were recorded for parent and Ru impregnated supports, with BET surface areas calculated over the relative pressure range 0.01-0.2. Pore diameters and volumes were calculated by applying the BJH method to desorption isotherms for relative pressures >0.35. Wide angle XRD patterns were recorded on a Bruker D8 Advance diffractometer with a Cu Kα (1.54 Á) source calibrated against a Si standard, between 2θ = 20-90 ° with a step size of 0.02 °. The Scherrer equation was used to calculate volume-averaged Ru particle sizes from line broadening, using the Ru (101) facet.[35] Low angle XRD patterns were recorded for 2θ = 0.5-2.5 ° with a step size of 0.02 °. Ru nanoparticle dispersion was measured via H_2 pulse chemisorption on a Quantachrome ChemBET3000 system, using the protocol reported by Tylus et al.[36] Catalysts were outgassed at 400 °C under 20 cm^3.min^{-1} flowing He for 1 h. Next, a pre-reduction step was employed at 400 °C under 10 cm^3.min^{-1} flowing hydrogen for 2 h. The sample cell was then purged under 20 cm^3.min^{-1} flowing He, prior to subsequent room temperature analysis. A $H_{(a)}$:Ru surface stoichiometry of 1 was assumed. This reduction protocol is comparable to that employed during initial catalyst synthesis and does not induce additional particle sintering and is sufficient to fully reduce the Ru NPs. Ru loading was determined by ICP-OES analysis on a Thermo Scientific iCAP-7000. High resolution high-angle annular dark-field STEM images were obtained on an aberration-corrected JEOL 2100-F microscope operated at 200 kV, with image analysis using ImageJ 1.41 software. Samples were dispersed in methanol and drop cast on 200-mesh carbon coated copper grids and dried under ambient conditions.

Furfural hydrogenation

Batch reaction conditions: Catalyst testing was performed using a stirred Parr 5513 100 cm^3 stainless steel autoclave (1000 rpm); precise control of hydrogen pressure and reaction temperature allowed for the elucidation of catalyst behaviour under varying operating conditions; isobaric operation was maintained throughout each reaction. Catalysts (50-100 mg) were added to reaction mixtures containing 10.86 mmol furfural, internal standard (dodecane, 0.3522 g) and toluene solvent (50 cm^3). Reactions were sampled periodically, via a dip-tube, for kinetic profiling by off-line gas chromatography using a Varian 450-GC with 8400 autosampler fitted with a (30 m x 0.25 mm x 0.25 μm) VF-5ms factor four column. The absolute Ru content varied between 0.83 μmol (for 0.08 wt% Ru/SiO_2 catalysts) and 101.67 μmol (for the highest loading 9.89 wt% Ru/SiO_2 catalysts), corresponding to substrate:Ru ratios ranging from 13067 (0.08 wt%) to 107 (9.89 wt%). Control experiments demonstrated negligible substrate conversion in the absence of H_2, support or ruthenium catalyst. Quoted activity and selectivity values are the mean of triplicate reactions with errors ± 3%; mass balances > 98% in all cases.

Conversion was calculated from **Equation 1**, where n_t is the number of mmol furfural at time t, and n_0 the initial mmol furfural, and selectivity calculated from **Equation 2** based exclusively on the six major liquid phase products, where nx=i is the mmol of product i (furfuryl alcohol, furan, methylfuran, 1,2-pentanediol, 1,5-pentanediol and tetrahydrofurfuryl alcohol) and Σnx denotes the total mmol of all products. Product yield was calculated from **Equation 3**. Mass-normalised initial rates were calculated from the first hour of reaction, and Turnover Frequencies (TOFs) calculated from **Equation 4** by normalising raw initial rates to the mmol surface Ru species determined from H_2 dispersion and HRTEM.

$$\% \text{ Conversion} = [(n_0 - n_t) / (n_0)] \times 100 \qquad \text{Equation 1}$$

$$\% \text{ Selectivity} = [(n_{x=i}) / (\Sigma n_x)] \times 100 \qquad \text{Equation 2}$$

$$\% \text{ Yield} = (\text{Conversion} \times \text{Selectivity}) / 100 \qquad \text{Equation 3}$$

$$\text{TOF} = \text{mmol}_{\text{Furfural}} \text{ converted.h}^{-1} / \text{mmol}_{\text{surface}} \text{ Ru} \qquad \text{Equation 4}$$

Acknowledgements

This work was supported by the EPSRC (EP/G007594/4, EP/K014749/1 and EP/K014676/1). We thank Professor Richard Palmer and Birmingham University for access to TEM facilities. This research has been supported (*in part*) by EU Marie-Curie IRSES EU-China Cooperation for Liquid Fuels from Biomass Pyrolysis (FP7-PEOPLE-2009-IRSES Grant 246772).

Keywords: Ruthenium • Furfural • Hydrogenation • Heterogeneous catalysis • Mesoporous silica

[1] a) J. Melorose, R. Perroy, S. Careas, in *Working Paper No. ESA/P/WP. 241*, **2015**, pp. 1-59; b) E. Kriegler, N. Bauer, A. Popp, F. Humpenöder, M. Leimbach, J. Strefler, L. Baumstark, B. L. Bodirsky, J. Hilaire, D. Klein, I. Mouratiadou, I. Weindl, C. Bertram, J.-P. Dietrich, G. Luderer, M. Pehl, R. Pietzcker, F. Piontek, H. Lotze-Campen, A. Biewald, M. Bonsch, A. Giannousakis, U. Kreidenweis, C. Müller, S. Rolinski, A. Schultes, J. Schwanitz, M. Stevanovic, K. Calvin, J. Emmerling, S. Fujimori, O. Edenhofer, *Glob. Environ. Chang.* **2017**, *42*, 297-315.

[2] a) M. J. Climent, A. Corma, S. Iborra, *Green Chem.* **2014**, *16*, 516-547; b) L. Yan, Q. Yao, Y. Fu, *Green Chem.* **2017**, *19*, 5527-5547.

[3] a) P. Kaparaju, M. Serrano, A. B. Thomsen, P. Kongjan, I. Angelidaki, *Bioresour. Technol.* **2009**, *100*, 2562-2568; b) V. Menon, M. Rao, *Prog. Energy Combust. Sci.* **2012**, *38*, 522-550.

[4] a) K. Wilson, A. F. Lee, *Philos. Trans. A: Math. Phys. Eng. Sci.* **2016**, *374*, 20150081; b) X. Zhang, K. Wilson, A. F. Lee, *Chem. Rev.* **2016**, *116*, 12328-12368.

[5] a) T. Werpy, G. Petersen, National Renewable Energy Lab., Golden, CO (US), **2004**; b) N. Sun, H. Rodriguez, M. Rahman, R. D. Rogers, *Chem. Commun.* **2011**, *47*, 1405-1421; c) A. Barakat, H. De Vries, X. Rouau, *Bioresour. Technol.* **2013**, *134*, 362-373.

[6] a) A. S. Mamman, J. M. Lee, Y. C. Kim, I. T. Hwang, N. J. Park, Y. K. Hwang, J. S. Chang, J. S. Hwang, *Biofuel. Bioprod. Biorefin.* **2008**, *2*, 438-454; b) R. Xing, W. Qi, G. W. Huber, *Energ. Environ. Sci.* **2011**, *4*, 2193-2205; c) P. Bhaumik, P. L. Dhepe, *ACS Catal.* **2013**, *3*, 2299-2303; d) Rodiansono, S. Khairi, T. Hara, N. Ichikuni, S. Shimazu, *Catal. Sci. Technol.* **2012**, *2*, 2139-2145.

[7] a) M. J. Taylor, L. J. Durndell, M. A. Isaacs, C. M. Parlett, K. Wilson, A. F. Lee, G. Kyriakou, *Appl. Catal. B* **2016**, *180*, 580-585; b) Á. O'Driscoll, J. Leahy, T. Curtin, *Catal. Today* **2017**, *279*, 194-201; c) M. Paniagua, J. Melero, J. Iglesias, G. Morales, B. Hernández, C. López-Aguado, *Appl. Catal. A* **2017**, *537*, 74-82.

[8] H.-Y. Zheng, Y.-L. Zhu, B.-T. Teng, Z.-Q. Bai, C.-H. Zhang, H.-W. Xiang, Y.-W. Li, *J. Mol. Catal. A* **2006**, *246*, 18-23.

[9] a) J. J. Bozell, L. Moens, D. Elliott, Y. Wang, G. Neuenscwander, S. Fitzpatrick, R. Bilski, J. Jarnefeld, *Resour. Conserv. Recy.* **2000**, *28*, 227-239; b) J. P. Lange, W. D. van de Graaf, R. J. Haan, *ChemSusChem* **2009**, *2*, 437-441.

[10] a) L. Bui, H. Luo, W. R. Gunther, Y. Román‐Leshkov, *Angew. Chem. Int.-Ed.* **2013**, *52*, 8022-8025; b) I. Delidovich, P. J. Hausoul, L. Deng, R. Pfützenreuter, M. Rose, R. Palkovits, *Chem. Rev.* **2015**, *116*, 1540-1599; c) M. Chalid, H. J. Heeres, A. Broekhuis, *Procedia Chem.* **2012**, *4*, 260-267.

[11] a) M. Choura, N. M. Belgacem, A. Gandini, *Macromolecules* **1996**, *29*, 3839-3850; b) L. Pranger, R. Tannenbaum, *Macromolecules* **2008**, *41*, 8682-8687.

[12] A. Mandalika, L. Qin, T. K. Sato, T. Runge, *Green Chem.* **2014**, *16*, 2480-2489.

[13] D. Liu, D. Zemlyanov, T. Wu, R. J. Lobo-Lapidus, J. A. Dumesic, J. T. Miller, C. L. Marshall, *J. Catal.* **2013**, *299*, 336-345.

[14] B. H. Wojcik, *Ind. Eng. Chem.* **1948**, *40*, 210-216.

[15] A. K. Shanker, C. Cervantes, H. Loza-Tavera, S. Avudainayagam, *Environ. Int.* **2005**, *31*, 739-753.

[16] R. V. Sharma, U. Das, R. Sammynaiken, A. K. Dalai, *Appl. Catal. A* **2013**, *454*, 127-136.

[17] a) V. V. Pushkarev, N. Musselwhite, K. An, S. Alayoglu, G. A. Somorjai, *Nano Lett.* **2012**, *12*, 5196-5201; b) S. H. Pang, J. W. Medlin, *ACS Catal.* **2011**, *1*, 1272-1283; c) W. Xu, H. Wang, X. Liu, J. Ren, Y. Wang, G. Lu, *Chem. Commun.* **2011**, *47*, 3924-3926.

[18] a) S. Sitthisa, T. Pham, T. Prasomsri, T. Sooknoi, R. G. Mallinson, D. E. Resasco, *J. Catal.* **2011**, *280*, 17-27; b) H. Li, H. Luo, L. Zhuang, W. Dai, M. Qiao, *J. Mol. Catal. A* **2003**, *203*, 267-275; c) P. Panagiotopoulou, D. G. Vlachos, *Appl. Catal. A* **2014**, *480*, 17-24; d) B. Nagaraja, A. Padmasri, B. D. Raju, K. R. Rao, *J. Mol. Catal. A* **2007**, *265*, 90-97.

[19] J. J. Musci, A. B. Merlo, M. L. Casella, *Catal. Today* **2017**, *296*, 43-50.

[20] R. M. Mironenko, O. B. Belskaya, T. I. Gulyaeva, A. I. Nizovskii, A. V. Kalinkin, V. I. Bukhtiyarov, A. V. Lavrenov, V. A. Likholobov, *Catal. Today* **2015**, *249*, 145-152.

[21] R. Huang, Q. Cui, Q. Yuan, H. Wu, Y. Guan, P. Wu, *ACS Sustainable Chem. Eng.* **2018**, *6*, 6957-6964.

[22] S. Sudiyarmanto, F. Aulia, F. Adzim, H. Setiyanto, A. A. Dwiatmoko, *AIP Conf. Proc.* **2018**, *2024*, 020027.

[23] a) J. Yang, J. Ma, Q. Yuan, P. Zhang, Y. Guan, *RSC Adv.* **2016**, *6*, 92299-92304; b) Q. Yuan, D. Zhang, L. v. Haandel, F. Ye, T. Xue, E. J. M. Hensen, Y. Guan, *J. Mol. Catal. A* **2015**, *406*, 58-64.

[24] C. Ramirez-Barria, M. Isaacs, K. Wilson, A. Guerrero-Ruiz, I. Rodríguez-Ramos, *Appl. Catal. A* **2018**, *563*, 177-184.

[25] D. Zhao, J. Feng, Q. Huo, N. Melosh, G. H. Fredrickson, B. F. Chmelka, G. D. Stucky, *Science* **1998**, *279*, 548-552.

[26] R. L. Clendenen, H. Drickamer, *J. Phys. Chem. Solids* **1964**, *25*, 865-868.

[27] W. Luo, U. Deka, A. M. Beale, E. R. van Eck, P. C. Bruijnincx, B. M. Weckhuysen, *J. Catal.* **2013**, *301*, 175-186.

[28] a) X. Zhang, L. J. Durndell, M. A. Isaacs, C. M. Parlett, A. F. Lee, K. Wilson, *ACS Catal.* **2016**, *6*, 7409-7417; b) C. M. Parlett, A. Aydin, L. J. Durndell, L. Frattini, M. A. Isaacs, A. F. Lee, X. Liu, L. Olivi, R. Trofimovaite, K. Wilson, *Catal. Commun.* **2017**, *91*, 76-79; c) L. J. Durndell, C. M. Parlett, N. S. Hondow, M. A. Isaacs, K. Wilson, A. F. Lee, *Sci. Rep.* **2015**, *5*, 9425; d) J. Morere, M. Tenorio, M. Torralvo, C. Pando, J. Renuncio, A. Cabanas, *J. Supercrit. Fluids* **2011**, *56*, 213-222; e) M. Opanasenko, P. Stepnicka, J. Cejka, *RSC Adv.* **2014**, *4*, 65137-65162.

[29] S. Xia, Y. Li, Q. Shang, C. Zhang, P. Ma, *Trans. Tianjin Univ.* **2016**, *22*, 202-210.

[30] S. Sitthisa, D. E. Resasco, *Catal. Lett.* **2011**, *141*, 784-791.

[31] D. Y. Murzin, *J. Catal.* **2010**, *276*, 85-91.

[32] S. Galvagno, G. Capannelli, G. Neri, A. Donato, R. Pietropaolo, *J. Mol. Catal.* **1991**, *64*, 237-246.

[33] S. Chen, R. Wojcieszak, F. Dumeignil, E. Marceau, S. Royer, *Chem. Rev.* **2018**, *118*, 11023-11117.

[34] A. M. Silva, O. A. A. Santos, M. J. Mendes, E. Jordão, M. A. Fraga, *Appl. Catal. A* **2003**, *241*, 155-165.

[35] I. Balint, A. Miyazaki, K.-i. Aika, *J. Catal.* **2003**, *220*, 74-83.

[36] J. Okal, M. Zawadzki, L. Kępiński, L. Krajczyk, W. Tylus, *Appl. Catal. A* **2007**, *319*, 202-209.

WILEY-VCH

Entry for the Table of Contents (Please choose one layout)

Layout 1:

FULL PAPER

Diverging apparent activation energies for furfural hydrogenation versus decarbonylation, enables optimisation of Ru nanoparticle size for selective furfuryl alcohol production.

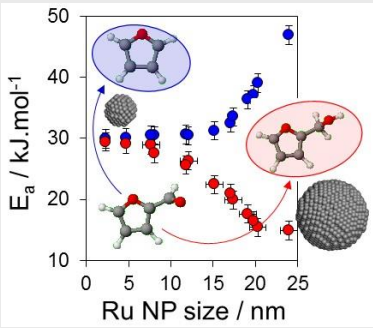

Lee J. Durndell,[a] Guchu Zou,[b] Wenfeng Shangguan,[b] Adam F. Lee[c] and Karen Wilson[c]*

Page No. – Page No.

Title

Layout 2:

FULL PAPER

((Insert TOC Graphic here; max. width: 11.5 cm; max. height: 2.5 cm))

*Author(s), Corresponding Author(s)**

Page No. – Page No.

Title

Text for Table of Contents